

Cite this article as: Wang Shuai, Liu Ying, Xu Dong, et al. Electrochemical Behavior of Pb-Co Anodes in Sulfuric Acid Electrolyte Containing Cl^- Ions[J]. Rare Metal Materials and Engineering, 2023, 52(05): 1565-1572.

ARTICLE

Electrochemical Behavior of Pb-Co Anodes in Sulfuric Acid Electrolyte Containing Cl^- Ions

Wang Shuai¹, Liu Ying¹, Xu Dong¹, Lin Wenjun², Wang Yong², Zhao Shuo¹, Yang Juan³, Zhou Xiangyang³

¹ School of Materials Science and Engineering, Hebei University of Engineering, Handan 056038, China; ² Zhuzhou Smelting Group Co., Ltd, Zhuzhou 412000, China; ³ School of Metallurgy and Environment, Central South University, Changsha 410083, China

Abstract: Pb-Co anodes with different Co contents (0.5wt%, 1wt%, and 2wt%) were prepared by powder metallurgy, and the traditional Pb-Ca-Sn anode was used as the reference for comparison. The electrochemical behavior of the anodes in the electrolyte containing 160 g/L H_2SO_4 and 500 mg/L Cl^- ions was evaluated by electrochemical measurements. The phase composition, surface morphologies, and element distribution of the anodic oxide layers after galvanostatic polarization for 72 h were investigated. With increasing the Co content, the anodic potential, charge transfer resistance, and oxygen evolution overpotential of the Pb-Co anodes are decreased gradually. After galvanostatic polarization for 72 h, the oxygen evolution overpotential of Pb-2wt% Co anode is lower than that of Pb-Ca-Sn anode by 101 mV. In addition, due to the presence of Cl^- ions, the charge transfer is improved, the oxygen evolution reaction is inhibited, and the oxide layer is deteriorated.

Key words: copper electrowinning; Pb-Co anode; oxygen evolution reaction; corrosion resistance; Cl^- ion

Copper, zinc, nickel, cobalt, manganese, and other non-ferrous metals can be smelted by hydrometallurgy and pyrometallurgy^[1-5]. Due to the advantages of high comprehensive utilization rate of resources, environmental protection of process, and strong adaptability to low grade ores, the hydrometallurgy is widely used in the extraction of the non-ferrous metals. The global reserves of nearly 20% copper, more than 85% zinc, most manganese, and almost 100% high-purity nickel/cobalt are extracted by hydrometallurgy^[6-10].

In copper hydrometallurgy, the copper electrowinning is an essential process, and Pb-Ca-Sn alloy is commonly served as an insoluble anode^[11-13]. Since the high electrocatalytic activity of Co is conducive to the oxygen evolution reaction (OER)^[14-16] and Co can inhibit the corrosion of Pb-based anode, a small amount of Co^{2+} ions are added into the electrolyte^[17-18]. Moreover, with increasing the Co^{2+} ions in electrolyte, the lead content in copper products and OER overpotential are decreased gradually^[19]. However, the high

cost of cobalt consumption in the copper electrowinning seriously restricts its application.

Therefore, the Pb-Co anodes are proposed and attract much attention for economical application. Compared with Pb anode, Pb-Co anode prepared by accumulative roll-bonding has better corrosion resistance, lower lead content in products, less anodic slime, and less energy consumption^[20]. When the Co content exceeds 0.5wt%, the corrosion resistance of Pb-Co anode is enhanced, and OER overpotential of Pb-3wt% Co anode is lower than that of Pb-1wt% Ag anode by about 90 mV^[21]. In addition, OER overpotential of Pb-Co and Pb-Co-Sn films is lower than that of the traditional Pb-Ca-Sn alloy by 68% and 55% in copper electrowinning, respectively^[22-23].

In the copper electrowinning industry, Cl^- ion usually exists in copper sulfate electrolyte, which may originate from the copper ore, production water, and chlorine additives for the amelioration of electrowinning process. When the electrolyte contains Cl^- ions, the electrochemical/chemical reactions

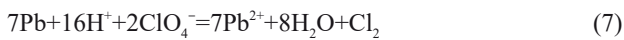
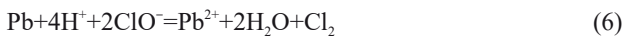
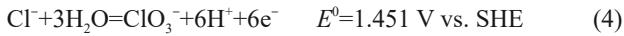
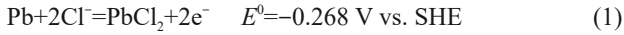
Received date: October 14, 2022

Foundation item: National Natural Science Foundation of China (51904085, 51904086, U20A20272); Supported by Zhuzhou Smelting Group Co., Ltd (ZYKJ20220408003); Natural Science Foundation of Hebei Province (E2021402056); Science and Technology Research and Development Program of Handan City (21422101235)

Corresponding author: Zhou Xiangyang, Ph. D., Professor, School of Metallurgy and Environment, Central South University, Changsha 410083, P. R. China, Tel: 0086-731-88836329, E-mail: xyzhou@csu.edu.cn

Copyright © 2023, Northwest Institute for Nonferrous Metal Research. Published by Science Press. All rights reserved.

occur on the Pb-based anode surface^[24], as follows:



It can be seen that the Cl^- ions not only accelerate the corrosion of Pb-based anode and shorten the service life of anode, but also reduce the quality of cathodic copper products^[25]. Moreover, the chlorine gas generated on the anode surface can further deteriorate the workshop environment when the electrolyte contains excess Cl^- ions.

The Pb-Co anode behavior in electrolyte containing Cl^- ions is rarely reported. Therefore, in this research, the Pb-Co anodes with different cobalt contents were produced by powder metallurgy. The oxygen evolution and corrosion behavior of Pb-Co anodes were investigated in sulfuric acid electrolyte containing 500 mg/L Cl^- ions. Meanwhile, the surface morphology, element distribution, and phase composition of anodic oxide layer were analyzed by scanning electron microscope (SEM), X-ray energy dispersive spectroscopy (EDS), and X-ray diffractometer (XRD), respectively. The reaction mechanism of Cl^- ions on Pb-Co anodic oxide layer was also discussed.

1 Experiment

Pb powder (Sinopharm Chemical Reagent Co., Ltd, China) and Co powder (Shanghai Aladdin Biotechnology Co., Ltd, China) were used as raw materials. The Pb powder of 0.5wt%, 1wt%, and 2wt% was mixed with Co powder in agate jar in argon atmosphere. Then, the mixed powder was treated by mechanical alloying at room temperature for 10 h through high energy planetary ball mill. Afterwards, the mixed powder was uniaxially compacted in a stainless-steel mold under 300 MPa. The compacts were sintered in a reducing furnace with hydrogen and argon mixture (volume ratio of $\text{H}_2:\text{Ar}=10:90$). The sintering process was as follows: (1) heating from room temperature to 300 °C at heating rate of 3 °C/min; (2) holding at 300 °C for 5 h; (3) cooling to room temperature. Fig. 1 shows the schematic diagram of mold and treatment process.

The obtained Pb-Co anodes were cut into cuboid specimens (10 mm×10 mm×5 mm) by wire cutting machine. Finally, the Pb-Co and Pb-Ca-Sn anodes were sealed by resin powder with a working area of 10 mm×10 mm and then connected to a plastic-isolated copper wire. The schematic diagram of assembled specimen is shown in Fig.2.

Before the electrochemical tests, the working surface of all the specimens was polished by SiC abrasive paper. The electrochemical workstation (PARSTAT 4000, Princeton, USA) was used to evaluate the electrochemical properties of the anodes in an electrolyte containing 160 g/L H_2SO_4 and 500 mg/L Cl^- ions at 45 °C. Considering that the anode reactions could hardly be affected by the cathode process, the copper

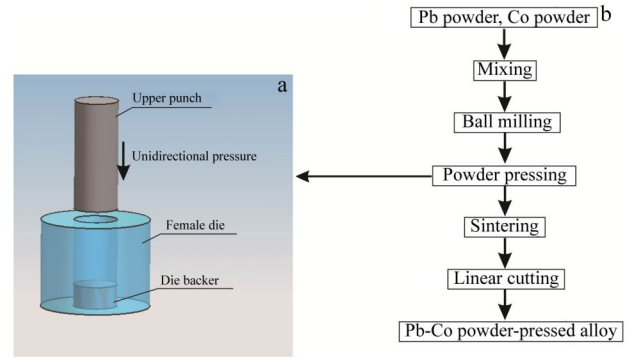


Fig.1 Schematic diagram of mold (a) and Pb-Co anode preparation process (b)

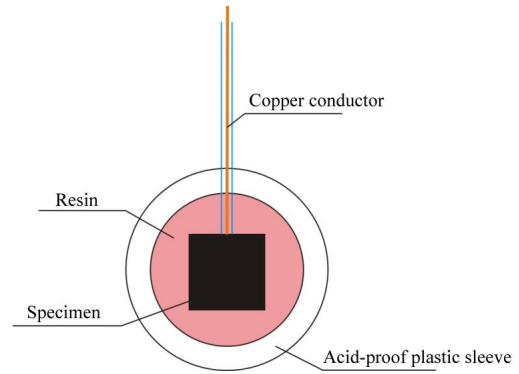


Fig.2 Schematic diagram of assembled anode specimen

sulphate was not added to the electrolyte for simplification. The counter electrode was platinum sheet (3 cm×3 cm), and the reference electrode was saturated Hg_2SO_4 electrode (0.645 V vs. MSE). The schematic diagram of three-electrode system is shown in Fig.3.

Cyclic voltammetry (CV) scanning was conducted at voltage from -1.4 V to 1.8 V with scanning rate of 20 mV/s. In order to obtain a stable anodic layer, the galvanostatic polarization was performed at current density of 200 A/m² for 72 h. Electrochemical impedance spectroscopy (EIS) was

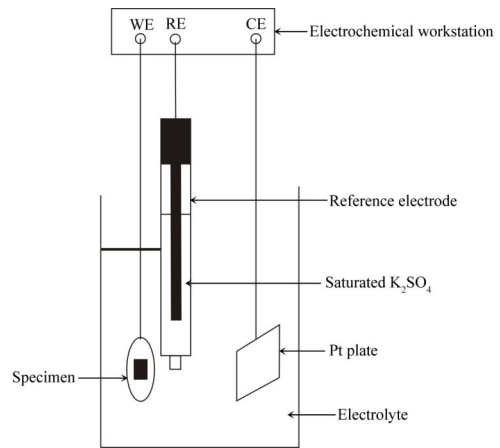


Fig.3 Schematic diagram of three-electrode system

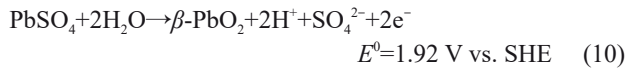
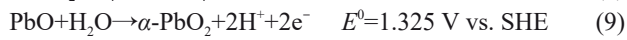
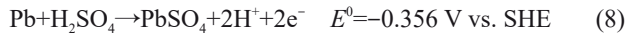
conducted at potential of 1.3 V with frequency of 0.01–100 kHz. Anodic polarization test was conducted at a sweep rate of 5 mV/s with the potential of 1.1–1.7 V.

After galvanostatic polarization, the anodes were taken out from the electrolyte, rinsed with deionized water, and air-dried. Then, the surface morphologies and phase composition of the anodic oxide layers were analyzed by SEM coupled with EDS (Quanta FEG250, American) and XRD (Rigaku-TTRIII, Japan).

2 Results and Discussion

2.1 CV curves

Fig.4 shows the CV curves of Pb-Co and Pb-Ca-Sn anodes at different potential ranges. According to the classical CV curve of the traditional Pb-based anode in sulfuric acid electrolyte, the electrochemical reactions corresponding to O1, O4, R1, R2, and R3^[26–27] are as follows:



Peak O1 corresponds to Eq. (8), presenting the oxidation from Pb to PbSO₄. Peak O4 corresponds to Eq. (9–11), presenting the oxidation from PbO to α-PbO₂, from PbSO₄ to β-PbO₂, and OER, respectively. Peak R1 corresponds to the reverse reaction of Eq. (9) and Eq. (10) during the negative scanning process. Peak R2 corresponds to the reduction

reaction from PbSO₄ and PbO into Pb. In addition, Peak R2 also corresponds to the reduction of some intermediate compounds (PbO·PbSO₄) to Pb^[20,28]. Peak R3 corresponds to the reduction reaction from PbSO₄ to Pb, i. e., the reverse reaction of Eq. (8), and hydrogen evolution reaction, namely Eq. (12). Moreover, the oxidation reactions of Eq. (2–5) are related to Peak O4 when the electrolyte contains Cl⁻ ions. Peak O2 may correspond to the oxidation reactions, namely Eq. (1) and Eq. (13). However, for the Pb-Co anodes, the appearance of Peak O3 may be attributed to the reaction in Eq. (14)^[29]. With increasing the Co content in Pb-Co anodes, the intensity of Peak O3 is gradually increased and Peak O3 shifts towards the positive direction.

On the one hand, the Peak O1, O3, O4, R2, and R3 of Pb-Co anodes are obviously higher than those of Pb-Ca-Sn anode, which indicates that the redox reactions on the oxide layer of Pb-Co anodes are more intense than those of Pb-Ca-Sn anode. This may be related to the fact that the electrochemical reaction occurs not only on the anode surface but also in the pores of Pb-Co anodes^[27,30]. On the other hand, compared with Pb-Ca-Sn anode, the O4 oxidation peak of Pb-Co anode is higher and moves towards the negative direction. This variation trend is more obvious with increasing the Co content, because Co promotes OER. The reaction mechanism^[29,31] is as follows:



Co is ionized in the electrolyte and forms the Co²⁺/Co³⁺ ion pairs. The reaction rate of Eq. (14) and Eq. (15) is higher than that of Eq. (10), and Co acts as the catalytic during OER process. However, the R1 reduction peak of Pb-Ca-Sn anode is much higher and shifts towards the negative direction, compared with those of the Pb-Co anodes. This may be attributed to the absorption of compounds corresponding to Eq. (14) on the Pb-Co anode surface, resulting in the easy reaction of SO₄²⁻ ions instead of Pb²⁺ ions^[32]. In addition, the cobalt compounds formed on the oxide layer surface not only promote OER, but also enhance the corrosion resistance of the anode.

2.2 Galvanostatic polarization

Fig.5 shows the galvanostatic polarization curves of the Pb-

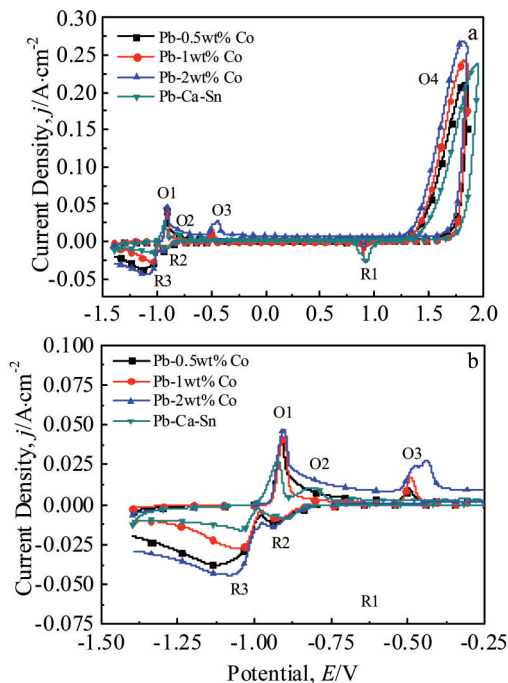


Fig.4 CV curves of Pb-Co and Pb-Ca-Sn anodes at potential $E = -1.5$ – 2.0 V (a) and $E = -1.50$ – -0.25 V (b)

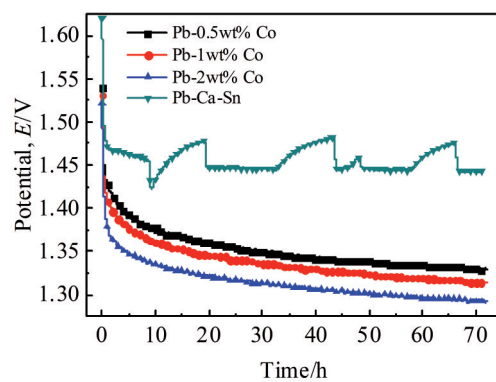


Fig.5 Galvanostatic polarization curves of Pb-Co and Pb-Ca-Sn anodes

Co and Pb-Ca-Sn anodes in the electrolyte containing 160 g/L H_2SO_4 and 500 mg/L Cl^- ions at current density of 200 A/m² for 72 h. It can be seen that the potential of all anodes is decreased rapidly and gradually becomes stable. The rapid decrease in potential is attributed to the conversion from $PbSO_4$ to PbO_2 on the anodic oxide layer, and the gradually stabilized potential is mainly related to the equilibrium between the formation and decomposition of oxide layer.

For Pb-Ca-Sn anode, the potential decreases rapidly at the beginning of galvanostatic polarization. After galvanostatic polarization for 9–20 h, the potential increases rapidly, then decreases, and finally becomes stable. After galvanostatic polarization for 20–72 h, three “serrated jump” phenomena appear and the potential finally reaches to 1.444 V.

The potential of Pb-Co anodes with different Co contents is much lower than that of the Pb-Ca-Sn anode in the whole galvanostatic polarization process. The potential decreases rapidly and then decreases slowly. As shown in Fig. 5, the stable potential of Pb-Co anodes is decreased gradually with increasing the Co content. After galvanostatic polarization for 72 h, the stabilized potentials of Pb-0.5wt% Co, Pb-1wt% Co, and Pb-2wt% Co anodes are 1.329, 1.313, and 1.292 V, which are lower than that of Pb-Ca-Sn anode by 115, 131, and 152 mV, respectively. Co is beneficial to reduce the activation energy of OER and can improve the electrocatalytic activity of the anodes, thus reducing the anodic potential^[33]. In addition, the large porosity and specific surface area of Pb-Co anodes result in their lower potential, compared with Pb-Ca-Sn anode.

In general, the potential change of Pb-Ca-Sn anode is quite different from that of Pb-Co anode. Compared with Ref.[34], the characteristic potential change of Pb-Ca-Sn anode in the electrolyte is caused by the strong corrosion effect of Cl^- ions,

which destroys the stable oxide layer and further oxidizes the anode substrate. The relatively slow potential change of the Pb-Co anodes indicates that the oxide layer is more stable and has better corrosion resistance, compared with the Pb-Ca-Sn anode. However, the continuous decrease in potential of Pb-Co anode in sulfuric acid electrolyte containing Cl^- ions is mainly attributed to the porous anode structure and strong corrosion effect of Cl^- ions, compared with the anode in sulfuric acid electrolyte. In addition, Cl^- ions may participate in the adverse reaction of chlorine evolution on the electrode surface, which consumes partial current and reduces polarization of OER.

2.3 EIS analysis

In order to investigate the electrochemical behavior and surface properties of the electrodes, EIS analysis of Pb-Co and Pb-Ca-Sn anodes was conducted, and the Nyquist curves and Bode diagrams are shown in Fig.6.

As shown in Fig.6a and 6c, all Nyquist diagrams present the single semicircle in the whole frequency region, indicating that the electrochemical reaction mechanism does not change with changing the anodes. The Bode plots (Fig. 6b and 6d) exhibit the single peak, suggesting that only one time constant exists. Therefore, the classical equivalent circuit model $R_s(R_1C)$ can be applied to simulate the electrochemical process of the anodes. R_s is the electrolyte resistance; R_1 is the charge transfer resistance; C is capacitance. Considering the frequency dispersion effect caused by the surface properties and roughness of anodes^[35], the perfect capacitance (C , interfacial capacitance) should be replaced by the constant phase element (CPE)^[36]. The impedance of CPE (Z_{CPE}) can be calculated by Eq.(17), as follows:

$$Z_{CPE} = \frac{1}{Q(j\omega)^n} \quad (17)$$

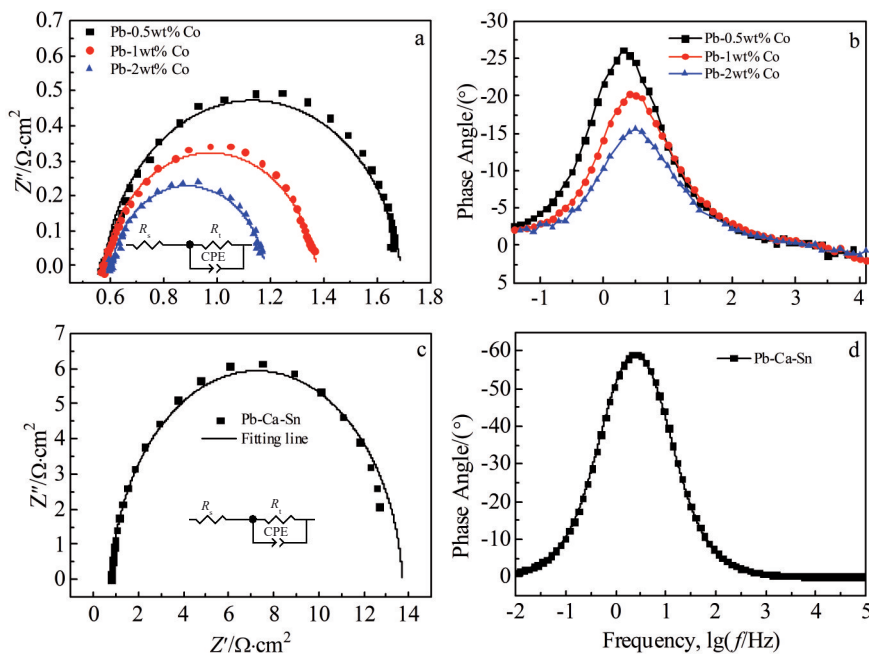


Fig.6 Nyquist diagrams (a, c) and Bode plots (b, d) of Pb-Co (a–b) and Pb-Ca-Sn (c–d) anodes

where Q is the capacity parameter related to the electrochemically active specific surface area exposed to the electrolyte; w denotes the angular frequency (rad/s); n represents the deviation degree ($n=0, 0.5, 1$ indicates the deviation from resistance, Warburg capacitance, and pure capacitance, respectively); j is the current density. The electrical double layer capacitance (C_{dl}) can be obtained by Eq.(18), as follows:

$$Q=(C_{dl})^n[(R_s)^{-1}+(R_t)^{-1}]^{(1-n)} \quad (18)$$

In the high frequency region of Nyquist plots, the intersection of the semicircle on the real Z' axis represents the electrolyte resistance R_s , and the diameter of the semicircles corresponds to the charge transfer resistance R_t of the electrode reaction. The experiment results are in good agreement with the fitting data, and the relevant parameters of the anodes are listed in Table 1.

As shown in Table 1, R_s values of all anodes are similar, whereas R_t differs between different anodes, indicating that OER is controlled by the charge transfer step, and the diffusion procedure has a little influence on OER. In addition, the R_t value of Pb-Co anodes is much lower than that of Pb-Ca-Sn anode, and it is decreased gradually with increasing the Co content. This is because Co is beneficial to promote the charge transfer of OER, and hence improves the electrocatalytic activity of the anode. However, the Q values of Pb-Co anodes are much higher than those of Pb-Ca-Sn anode, suggesting that Pb-Co anodes have a larger active surface area for electrochemical reactions^[37]. Compared with those in the pure sulfuric acid electrolyte^[38], the R_t value of anodes in the electrolyte containing Cl^- ions is smaller and the Q value is larger, indicating that Cl^- ions participate in the electrochemical reaction and promote the charge transfer of the anodes. The n values of all anodes are lower than 1, and the n value and phase angle are decreased gradually with

increasing the Co content (Fig.6b), indicating that C_{dl} deviates from the ideal capacitance. Particularly, the C_{dl} values of Pb-Co anodes with the presence of Cl^- ions in electrolyte are lower than those in the electrolyte without Cl^- ions. This may be because Cl^- ions reduce the OER active sites on the anodic surface.

2.4 Anodic polarization curves

In order to investigate the oxygen evolution behavior of the anodes, the anodic polarization curves were measured after galvanostatic polarization test, and the results are shown in Fig.7a. It can be seen that the current density of all anodes is increased gradually with increasing the potential, and the potential is decreased gradually with increasing the Co content.

OER overpotential (η) of the anodes is corrected^[9,39] by Eq.(19), as follows:

$$\eta=E-1.229+0.64-iR_s \quad (19)$$

where E is the actual potential; 1.229 represents the equilibrium potential of OER; 0.64 represents MSE potential; i is exchange current density. Meanwhile, the electrochemical parameters (a, b) and the exchange current density i of the anodes can be calculated by linear fitting of R_s -corrected results and Tafel equation ($\eta=a+blgi$, when $\eta=0$), respectively. The related electrochemical parameters are listed in Table 2. According to Fig.7b, OER overpotential of different anodes can be arranged in order: Pb-Ca-Sn>Pb-0.5wt% Co>Pb-1wt% Co>Pb-2wt% Co.

According to Ref. [40–41], OER mechanism consists of several steps, as follows:



where S is the active site on the anodic oxide layer surface;

Table 1 Equivalent circuit parameters of Pb-Co and Pb-Ca-Sn anodes

Anode	Electrolyte resistance, $R_s/\Omega \cdot cm^2$	Charge transfer resistance, $R_t/\Omega \cdot cm^2$	Capacity, $Q/\times 10^{-2} \Omega^{-1} \cdot cm^{-2} \cdot s^n$	Deviation degree, n	Electrical double layer capacitance, $C_{dl}/\mu F \cdot cm^{-2}$
Pb-0.5wt% Co	0.579	1.11	14.027	0.907	10 386.55
Pb-1wt% Co	0.579	0.794	14.179	0.871	9 028.67
Pb-2wt% Co	0.606	0.575	17.562	0.859	10 803.40
Pb-Ca-Sn	0.773	12.95	2.422	0.948	19 410.09

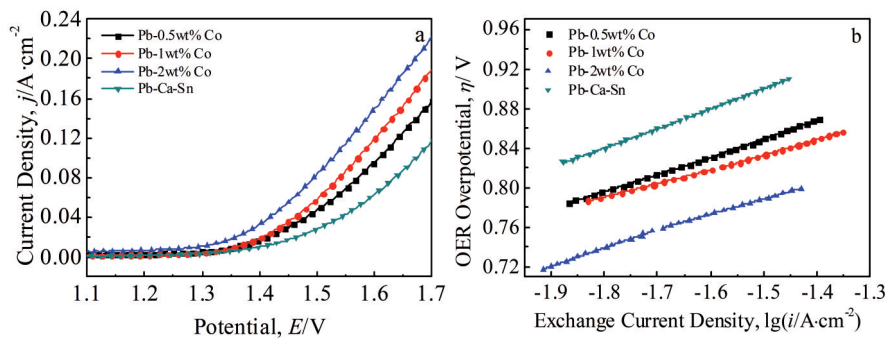


Fig.7 Anodic polarization curves (a) and R_s -corrected results (b) of Pb-Co and Pb-Ca-Sn anodes

$S\text{-OH}_{\text{ads}}$ and $S\text{-O}_{\text{ads}}$ represent two adsorbed intermediates. Among the four steps, the control step of OER rate depends on the Tafel slope. According to Table 2, all Tafel values are greater than 0.12 V/dec, indicating that Eq.(20) is the control step of OER rate.

Generally, the copper electrowinning is conducted at high current density. Thus, the kinetic parameters of OER at high overpotential can be used to assess the electrocatalytic activity of electrode. As shown in Table 2, the a_2 value is decreased gradually with increasing the Co content, suggesting that Co is beneficial to improve OER kinetics and electron transfer. Because the $\text{Co}^{2+}/\text{Co}^{3+}$ ion pairs and/or cobalt compounds are beneficial to increase the active sites on the anodic oxide layer with low energy barrier, the formation and adsorption of $S\text{-OH}_{\text{ads}}$ is enhanced and the electrocatalytic activity of OER is improved^[42]. These results also lead to the low b_2 value for the Pb-Co anodes. Besides, the η value of Pb-0.5wt% Co, Pb-1wt% Co, and Pb-2wt% Co anodes is 0.813, 0.804, and 0.759 V at 200 A/m², which is lower than that of the Pb-Ca-Sn anode by 47, 56, and 101 mV, respectively. Compared with those of the sulfuric acid electrolyte without Cl^- ions^[38], the larger b and η values of the sulfuric acid electrolyte with Cl^- ions indicate that Cl^- ions can inhibit OER.

2.5 XRD analysis of anodic oxide layer

XRD characterization was conducted to study the phase composition of the oxide layer formed on the Pb-Co and Pb-Ca-Sn anodes after galvanostatic polarization test, as shown in

Fig. 8. The oxide layer of Pb-Co anodes mainly consists of PbSO_4 , $\alpha\text{-PbO}_2$, $\beta\text{-PbO}_2$, Pb, and CoS.

As shown in Fig. 8, the diffraction peaks of $\alpha\text{-PbO}_2$ phase at $2\theta=23.25^\circ$, 50.55° , 55.86° corresponding to (110), (221), and (113) planes, respectively, and their intensities are increased with increasing the Co content, which is attributed to the improvement of bonding force and stability for anodic oxide layer. In addition, with increasing the Co content in anodes, the peak intensities of $\beta\text{-PbO}_2$ phase at $2\theta=25.43^\circ$ and $2\theta=31.97^\circ$, which correspond to (110) and (101) planes, respectively, are also increased with increasing the Co content in anodes, suggesting that the electrocatalytic ability and OER activity of anodic oxide layer is enhanced^[43]. The diffraction peaks of CoS phase at $2\theta=33.81^\circ$, 43.56° , 53.21° , 62.79° , and 64.30° correspond to (101), (102), (110), (112), (004) planes, respectively. The peak intensities are increased with increasing the Co content in anodes. These results all lead to the low OER overpotential. However, the appearance of Pb diffraction peak may be related to the porosity of the anodes or the strong corrosion effect of Cl^- ions^[44].

2.6 Surface morphologies of anodic oxide layer

Fig.9 shows the surface morphologies of oxide layers on Pb-0.5wt% Co, Pb-1wt% Co, and Pb-Ca-Sn anodes after galvanostatic polarization for 72 h. SEM morphologies and EDS element distributions of Pb-2wt% Co anode are shown in Fig. 10. Significant changes can be observed with different anodes.

Table 2 Overpotentials and electrochemical parameters of OER of Pb-Co and Pb-Ca-Sn anodes

Anode	a_1	b_1	a_2	b_2	$i_1/\text{A}\cdot\text{cm}^{-2}$	$i_2/\text{A}\cdot\text{cm}^{-2}$	η/V ($i=0.02\text{ A}\cdot\text{cm}^{-2}$)
Pb-0.5wt% Co	1.103	0.170	1.138	0.192	3.25×10^{-7}	1.18×10^{-6}	0.813
Pb-1wt% Co	1.036	0.136	1.070	0.158	2.41×10^{-8}	1.69×10^{-7}	0.804
Pb-2wt% Co	1.076	0.187	1.019	0.153	1.76×10^{-6}	2.19×10^{-7}	0.759
Pb-Ca-Sn	1.188	0.194	1.208	0.205	7.52×10^{-7}	1.28×10^{-6}	0.860

As displayed in Fig.9c, the surface micromorphology of the oxide layer formed on the Pb-Ca-Sn anode is mainly composed of orthorhombic crystals, tetragonal crystals, and some amorphous fine particles. Some holes can be observed in grains, which may be related to OER and the corrosion effect of Cl^- ions. It is worth noting that the porous oxide layer is loosely attached to the anode surface and it easily falls off, resulting in the further corrosion of anode. For the Pb-0.5wt% Co anode (Fig.9a), the anodic oxide layer consists of orthorhombic crystals, tetragonal crystals, and more amorphous fine particles, compared with those in Pb-Ca-Sn anode, suggesting that the crystal grains are refined. As for the Pb-1wt% Co anode (Fig.9b), the crystal grain size is further decreased and the anodic oxide layer becomes denser. The oxide layer of Pb-2wt% Co anode is hard, flat, and compact, resulting in the slowest corrosion rate.

With increasing the Co content, the crystal grain size is decreased, and the surface flatness/compactness is improved. Besides, the Pb, O, S, and Co elements are uniformly distributed on the surface of oxide layer, which is consistent

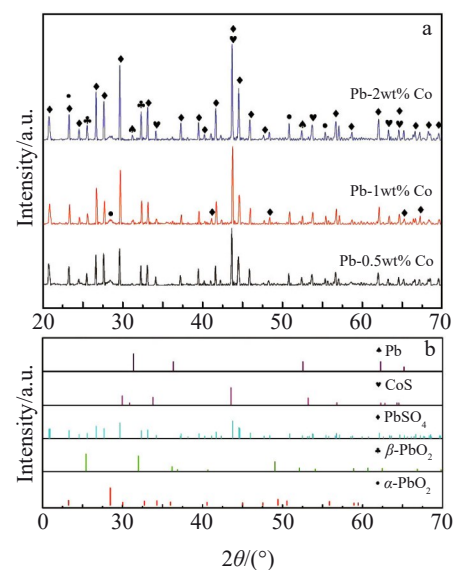


Fig.8 XRD patterns of oxide layer on Pb-Co anodes after galvanostatic polarization (a) and composition reference (b)

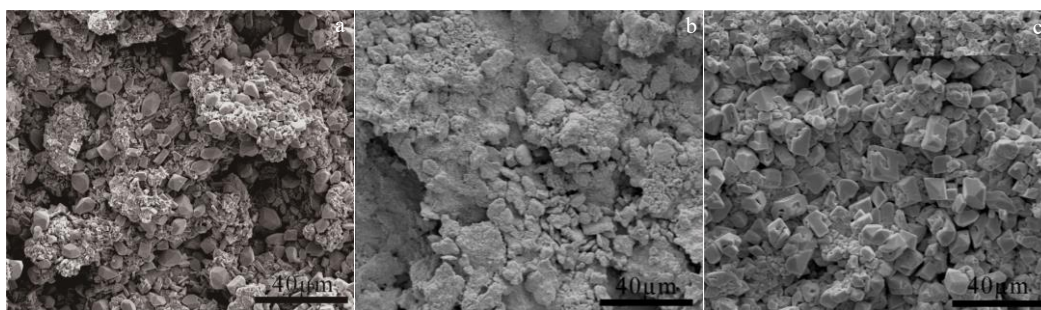


Fig.9 SEM morphologies of Pb-0.5wt% Co (a), Pb-1wt% Co (b), and Pb-Ca-Sn (c) anodes after galvanostatic polarization for 72 h

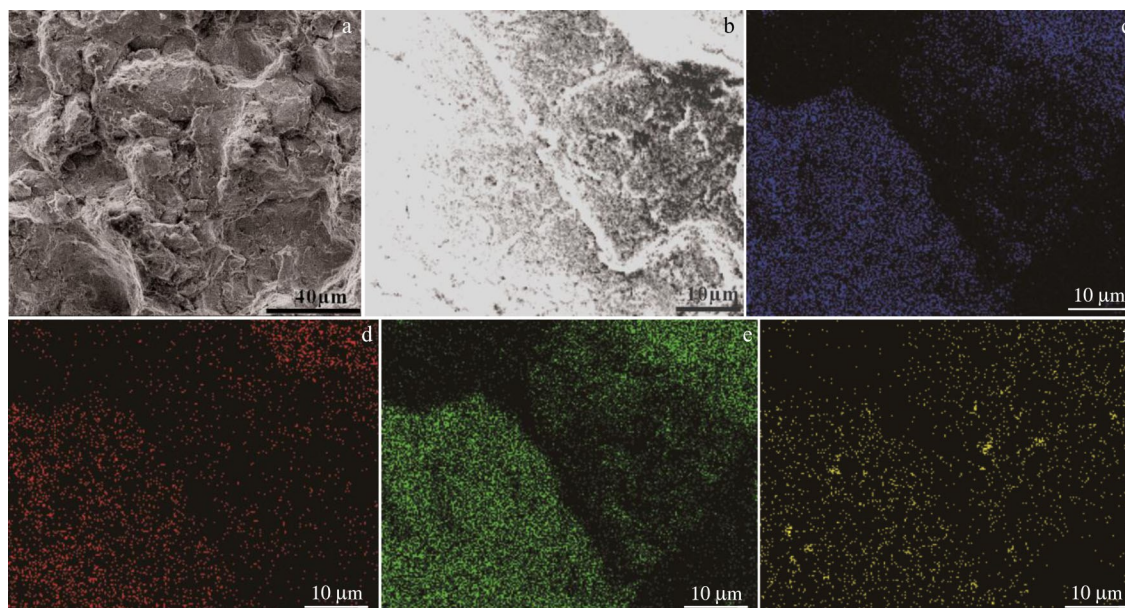


Fig.10 SEM morphologies (a–b) and EDS element distributions of Pb (c), O (d), S (e), and Co (f) in Pb-2wt% Co anode

with XRD results. The cobalt compounds as well as fine crystal grains increase the oxygen evolution active sites on the anode surface and reduce the driving force of OER. All these results suggest that the chloride ions can inhibit the formation of anodic surface film and accelerate the corrosion of anode^[38].

3 Conclusions

1) With increasing the Co content in the anode, the anodic potential, charge transfer resistance, and oxygen evolution reaction (OER) overpotential of the Pb-Co anodes are gradually decreased. After galvanostatic polarization for 72 h, the OER overpotential of Pb-2wt% Co anode is lower than that of Pb-Ca-Sn anode by about 101 mV, because the $\text{Co}^{2+}/\text{Co}^{3+}$ ion pairs and/or cobalt compounds improve the electrocatalytic activity of OER.

2) With increasing the Co content in the anode, the crystal grain size of the anodic oxide layer is decreased, while the surface flatness and compactness are increased gradually, indicating that the corrosion resistance of the anode is enhanced.

3) The Cl^- ions in the electrolyte participate in the electrochemical reaction, promote the charge transfer, but

inhibit OER, reduce the active site of OER, deteriorate the anodic oxide layer, and accelerate the corrosion of anode. The Pb-2wt% Co anode exhibits the optimal electrocatalytic activity and corrosion resistance, showing a promising application for copper electrowinning.

References

- 1 Habashi F. *Journal of Mining and Metallurgy-Section B: Metallurgy*[J], 2007, 43(1): 1
- 2 Wang J, Zhang Y Y, Cui K K et al. *Journal of Cleaner Production*[J], 2021, 298: 126 788
- 3 Geoffrey S, Sehliselo N, Lubinda F. *Hydrometallurgy*[J], 2010, 103(1–4): 150
- 4 Wang S J. *JOM*[J], 2006, 58(10): 47
- 5 Liu B B, Zhang Y B, Lu M M et al. *Minerals Engineering*[J], 2019, 131: 286
- 6 Clancy M, Bettles C, Stuart A et al. *Hydrometallurgy*[J], 2013, 131–132: 144
- 7 Antuñano N, Herrero D, Arias P et al. *Process Safety and Environmental Protection*[J], 2013, 91(6): 495

- 8 Zhang C, Liu J H, Chen B M. *Ceramics International*[J], 2018, 44(16): 19 735
- 9 Chen S, Chen B M, Wang S C et al. *Journal of Alloys and Compounds*[J], 2020, 815: 152 551
- 10 Peek E, Åkre T, Asselin E. *JOM*[J], 2009, 61: 43
- 11 Yuan X T, Lv X D, Hua Z Q et al. *Advanced Materials Research*[J], 2012, 402: 349
- 12 Wang S, Liu Y, Xu D et al. *Rare Metal Materials and Engineering*[J], 2022, 51(6): 1986
- 13 Cifuentes L, Montes A, Crisóstomo G. *Corrosion Engineering, Science and Technology*[J], 2011, 46: 737
- 14 Shi L N, Cui L T, Ji Y R et al. *Coordination Chemistry Reviews*[J], 2022, 469: 214 668
- 15 Chang H, Shi L N, Chen Y H et al. *Coordination Chemistry Reviews*[J], 2022, 473: 214 839
- 16 Chang H, Li X Z, Shi L N et al. *Chemical Engineering Journal*[J], 2021, 421(Part 1): 129 944
- 17 Nikoloski A N, Nicol M J. *Mineral Processing and Extractive Metallurgy Review*[J], 2007, 29(2): 143
- 18 Panda B, Das S C, Panda R K. *Hydrometallurgy*[J], 2009, 95(1-2): 87
- 19 Zhang Y C, Guo Z C. *Journal of Alloys and Compounds*[J], 2019, 780: 131
- 20 Karbasi M, Alamdari E K, Dehkordi E A. *Hydrometallurgy*[J], 2019, 183: 51
- 21 Rashkov S, Dobrev T, Noncheva Z et al. *Hydrometallurgy*[J], 1999, 52(3): 223
- 22 Maril M, Tobosque P, Núñez J et al. *Materials Characterization*[J], 2019, 148: 323
- 23 Maril M, Tobosque P, Cisternas N et al. *Journal of the Electrochemical Society*[J], 2021, 168(5): 52 505
- 24 Lashgari M, Hosseini F. *Journal of Chemistry*[J], 2013, 2013: 538 462
- 25 Wang S, Zhou X Y, Ma C Y et al. *Hydrometallurgy*[J], 2018, 177: 218
- 26 Zhang Y C, Guo Z C. *Journal of Alloys and Compounds*[J], 2017, 724: 103
- 27 Mohammadi M, Mohammadi F, Alfantazi A. *Journal of the Electrochemical Society*[J], 2013, 160(4): E35
- 28 Schmachtel S, Toiminen M, Kontturi K et al. *Journal of Applied Electrochemistry*[J], 2009, 39: 1835
- 29 Ivanov I, Stefanov Y. *Hydrometallurgy*[J], 2002, 64(2): 111
- 30 Ravindran K, Heerman L, Van Simaey L. *Bulletin des Sociétés Chimiques Belges*[J], 1974, 83(5-6): 173
- 31 Ivanov I, Stefanov Y, Noncheva Z et al. *Hydrometallurgy*[J], 2000, 57(2): 109
- 32 Nakayama M, Fujimoto K, Kobayakawa T et al. *Electrochemistry Communications*[J], 2017, 84: 24
- 33 Huang H, Zhou J Y, Guo Z C. *Transactions of Nonferrous Metals Society of China*[J], 2010, 20(S1): s55
- 34 Yang H T, Guo Z C, Chen B M et al. *Hydrometallurgy*[J], 2014, 147-148: 148
- 35 Lebrini M, Fontaine G, Gengembre L et al. *Corrosion Science*[J], 2009, 51(6): 1201
- 36 Zhou X Y, Ma C Y, Yang J et al. *Rare Metal Materials and Engineering*[J], 2018, 47(10): 3008
- 37 Yao Z P, Jiang Z H, Wang F P. *Electrochimica Acta*[J], 2007, 52(13): 4539
- 38 Wang S, Zhou X Y, Ma C Y et al. *RSC Advances*[J], 2018, 8(25): 13 910
- 39 Wang X B, Wang J L, Jiang W H et al. *Separation and Purification Technology*[J], 2021, 272: 118 916
- 40 Cao J L, Zhao H Y, Cao F H et al. *Electrochimica Acta*[J], 2007, 52(28): 7873
- 41 Li Y, Jiang L X, Liu F Y et al. *RSC Advances*[J], 2014, 4(46): 24 024
- 42 Bi Y M, Cai Z, Zhou D J et al. *Journal of Catalysis*[J], 2018, 358: 100
- 43 Yang H T, Chen B M, Liu H R et al. *International Journal of Hydrogen Energy*[J], 2014, 39(7): 3087
- 44 Lai Y Q, Li Y, Jiang L X et al. *Journal of Electroanalytical Chemistry*[J], 2012, 671: 16

Pb-Co 阳极在含氯硫酸电解液中的电化学行为

王 帅¹, 刘 颖¹, 徐 东¹, 林文军², 王 勇², 赵 烁¹, 杨 娟³, 周向阳³

(1. 河北工程大学 材料科学与工程学院, 河北 邯郸 056038)

(2. 株洲冶炼集团有限公司, 湖南 株洲 412000)

(3. 中南大学 冶金与环境学院, 湖南 长沙 410083)

摘 要: 采用粉末冶金法制备了不同Co含量(0.5%, 1.0%, 2.0%, 质量分数)的Pb-Co阳极, 并与传统的Pb-Ca-Sn阳极进行了对比试验。通过电化学测试研究了阳极在160 g/L H₂SO₄、500 mg/L Cl⁻电解液中的电化学行为, 研究了恒电流极化72 h后阳极氧化层的物相组成、表面形貌和元素分布。随着Co含量的增加, Pb-Co阳极的电位、电荷传递电阻和析氧过电位逐渐降低。恒电流极化72 h后, Pb-2%Co阳极的析氧过电位比Pb-Ca-Sn阳极低101 mV。此外, 在Cl⁻的存在下, 电荷传递得到改善, 析氧反应受到抑制, 阳极氧化层恶化。
关键词: 铜电积; Pb-Co阳极; 析氧反应; 耐腐蚀性能; 氯离子

作者简介: 王 帅, 男, 1988年生, 博士, 副教授, 河北工程大学材料科学与工程学院, 河北 邯郸 056038, E-mail: wangshuai@hebeu.edu.cn